International Journal of Remote Sensing, 2013
Vol. 34, No. 21, 7811–7820, http://dx.doi.org/10.1080/01431161.2013.822595

Effects of noise on optimal deconvolution accuracy in microwave observations

Ashutosh S. Limaye[a]*, William L. Crosson[b], and Charles A. Laymon[b]

[a]*NASA Marshall Space Flight Center/ZP11, Huntsville, AL 35805, USA;* [b]*Universities Space Research Association, Huntsville, AL 35805, USA*

(*Received 4 May 2012; accepted 22 June 2013*)

Due to large footprints of remotely sensed microwave brightness temperatures, accuracy of microwave observations in areas of large surface heterogeneity has always been a technological challenge. Microwave observations in areas dominated by waterbodies typically exhibit observed brightness temperature several tens of kelvins lower than areas having no surface water. The non-linearity between brightness temperature and other geophysical quantities such as soil moisture makes the accuracy of microwave observations a critical element for accurate estimation of these quantities. In retrieving soil moisture estimates, an error of 1 K in remotely sensed microwave brightness temperatures results in about 0.5–1% error in volumetric soil moisture. Large uncertainties in the observed brightness temperatures make such observations unusable in areas of large brightness temperature contrast. In this article, we discuss a deconvolution method to improve accuracy using the overlap in the adjacent microwave observations. We have shown that the method results in improved accuracy of 40% in brightness temperature estimation in regions of high brightness temperature contrast.

1. Introduction

Optimal deconvolution (ODC) of remotely sensed microwave brightness temperature (T_B) results in improved accuracy when compared to conventional estimation techniques (Limaye et al. 2004; Limaye, Crosson, and Laymon 2006). Typically, microwave observations have significant spatial overlap among adjacent observations. ODC relies on that overlap to accurately deconvolve Earth grid T_Bs. Previously, the authors had shown that synthetically constructed remotely sensed observations can be better reproduced by the ODC technique than by the conventional averaging technique. However, these studies did not account for calibration errors or instrument noise. Typically, instrument noise is white in nature (Bauer and Bennartz 1998) with a mean of 0 and a standard deviation (SD) ranging from 0–2 K. The noise is of similar magnitude to the difference among adjacent observations, on which the technique depends for deconvolution. Therefore, instrument noise results in what is commonly referred to as 'noise amplification'. In this article, we present an analysis of synthetic data sets which utilize the ODC technique combined with a footprint-matching technique to increase the overall accuracy of estimated Earth grid T_Bs in the presence of instrument noise.

*Corresponding author. Email: Ashutosh.Limaye@nasa.gov

Stogryn (1978) applied the Backus–Gilbert Method (BGM) to microwave observations to examine trade-offs between spatial resolution and noise. This is an optimal interpolation technique which uses adjacent observations to produce a synthetic observation at a given location. The weights for the adjacent observations are derived in an optimal way to match the antenna footprint pattern of the observation at that location. Stogryn's approach has been used extensively for a number of applications, including spatial resolution enhancements (Farrar and Smith 1992; Robinson, Kummerow, and Olson 1992) and antenna pattern matching and convolutions (Poe 1990; Bauer and Bennartz 1998; Mo 1999; Bennartz 2000; Stephens and Jones 2002). Several of these studies have identified sensor noise amplification as a source of error for optimal interpolation techniques. Noise is an unavoidable component of microwave observations. It is a function of the observation integration time, thermal gradients across the antenna, instrument noise, stability of the calibration loads, and out-of-band bleed. Typically, the variance of the noise is quantified using the instrument's pre-launch characterization. Noise in observations results in significant degradation of accuracy in deconvolution (Bauer and Bennartz 1998). Here, we present the effects of sensor noise on Earth grid T_B in the context of optimal deconvolution. BGM can be effectively used to trade instrument noise with spatial resolution enhancement (Bauer and Bennartz 1998; Stephens and Jones 2002, 2007). However, the effects of noise have not been documented in so far as T_B comparisons to a known Earth grid are concerned.

The ODC method utilizes the significant antenna pattern overlap to reduce sensor noise amplification. In order to quantify the utility of such a technique, we generated a synthetic grid of Earth grid T_B at high spatial resolution. This grid serves as the original T_B for subsequent comparisons and tests of estimation accuracy. These T_Bs were convolved using a surrogate antenna pattern for a planned NASA satellite microwave instrument, Soil Moisture Active Passive (SMAP), to simulate the actual observations from a space-borne sensor. We added random noise to each observation to simulate realistic observations from space. We applied BGM to these observations to match the antenna pattern (or antenna response function) using the adjacent beam positions. The BGM-reconstructed observations were then used in optimal deconvolution to produce Earth grid estimates. The reason we chose to perform this analysis using synthetic data sets was to assess the improvement in accuracy using this technique. Since the analysis uses the synthetic T_B, the true (or original) Earth grid T_B is known. The deconvolved T_B can be compared against the true T_B to evaluate the improvement compared with the grid T_B estimated using the conventional technique.

2. Optimal deconvolution

For a space-based microwave radiometer, the size of the Earth grid chosen on which the observations are mapped is much smaller than the half-power beamwidth. If the Earth grid is relatively coarse and the sampling rate is high, as anticipated in the case of SMAP, several observations are centred in a given Earth grid cell. Conventionally, these multiple T_B observations within each grid cell are averaged to produce the Earth grid estimate (referred to hereafter as conventional averaging, CA). Because a significant portion of the observed signal is derived from contribution outside of the grid cell, the resulting T_B map exhibits significant smoothing, especially in regions with high T_B contrasts, such as coastlines or areas with large waterbodies. A brief summary of the optimal deconvolution technique is presented below.

Brightness temperature at a given Earth location ρ_0 (centre of the footprint) can be given as

$$\hat{T}_{\mathrm{B}}(\rho_0) = \int_{\rho_0\,\mathrm{FOV}} \mathrm{G}(\rho_0) T_{\mathrm{B}}(A)\mathrm{d}A, \tag{1}$$

$$\mathrm{Min}\left|\hat{T}_{\mathrm{B}}(\rho_0) - T_{\mathrm{B}}(\rho_0)\right|_E, \tag{2}$$

where G is the antenna response function and E is its spatial extent of the field of view (FOV) of the observation. Sensors measure the $T_{\mathrm{B}}(\rho_0)$, whereas $T_{\mathrm{B}}(A)$ is the brightness temperature at the Earth grid, the quantity of interest in this analysis. The overlap among adjacent observations is significant in Equation (1) because each of the adjacent, overlapping observations provides a sufficient number of equations to solve for the unknown quantity, Earth grid T_{B}. Least squares optimization is used to solve the system of equations to minimize Equation (2) in a cumulative error form. The result is reduction in errors in the Earth grid T_{B}, which is discussed in more detail in the later section.

2.1. *Backus–Gilbert method*

Application of BGM to noisy observations is a standard practice (Ashcroft and Wentz 2004) and can be used to enhance spatial resolution or to reduce the noise in the data (Stephens and Jones 2002). In this article, we have used it for noise reduction. The basic thesis of BGM is that adjacent noisy observations can be used to reconstruct an observation with less noise at any given location. Consider a set of $i = 1$–N brightness temperature observations ($T_{\mathrm{B}i}$) with known antenna gain patterns. The T_{B} at any location (ρ_0) in the field of view of these observations can be estimated using

$$\hat{T}_{\mathrm{B}}(\rho_0) = \sum_{i=1}^{N} a_i T_{Ai} = \int_{\rho_0\mathrm{FOV}} \sum_{i=1}^{N} a_i G_i(\rho) T_{\mathrm{B}}(\rho)\mathrm{d}A. \tag{3}$$

However, before Equation (3) can be used to estimate the noise-reduced observations ($\hat{T}_{\mathrm{B}}(\rho_0)$, hereafter called BGM observations), we need to estimate the BGM weighting coefficients a_i. Estimation of these coefficients is critical for accurate representation of the antenna pattern at location ρ_0. Antenna pattern matching can be achieved by minimizing the difference in the matched and original antenna pattern, as follows.

$$Min \int_{\rho_0\mathrm{FOV}} \left[\mathrm{G}(\rho_0) - \sum_{i=1}^{N} a_i G_i(\rho)\right], \tag{4}$$

where

$$\sum_{i=1}^{N} a_i = 1. \tag{5}$$

It is expected that BGM observations will result in significant improvements in error statistics.

2.2. Study area and generation of synthetic SMAP observations

Brightness temperatures on an Earth grid cannot be independently measured. Therefore, we established a synthetic observation set in order to quantify the errors associated with the CA technique or the improvements brought by the combined BGM–ODC approach. In our previous studies, we characterized the ODC improvements over a large domain in the US Upper Midwest (Figure 1). The study area includes Lake Superior in the north along with the adjacent forest, an area with high T_B contrast. The southern region is mostly pastureland and row crops, and has a lower T_B contrast. A radiative transfer model was used to simulate L band T_Bs at a 1 km grid resolution based on vegetation types defined by the National Land Cover Dataset (NLCD). These data serve our need for a

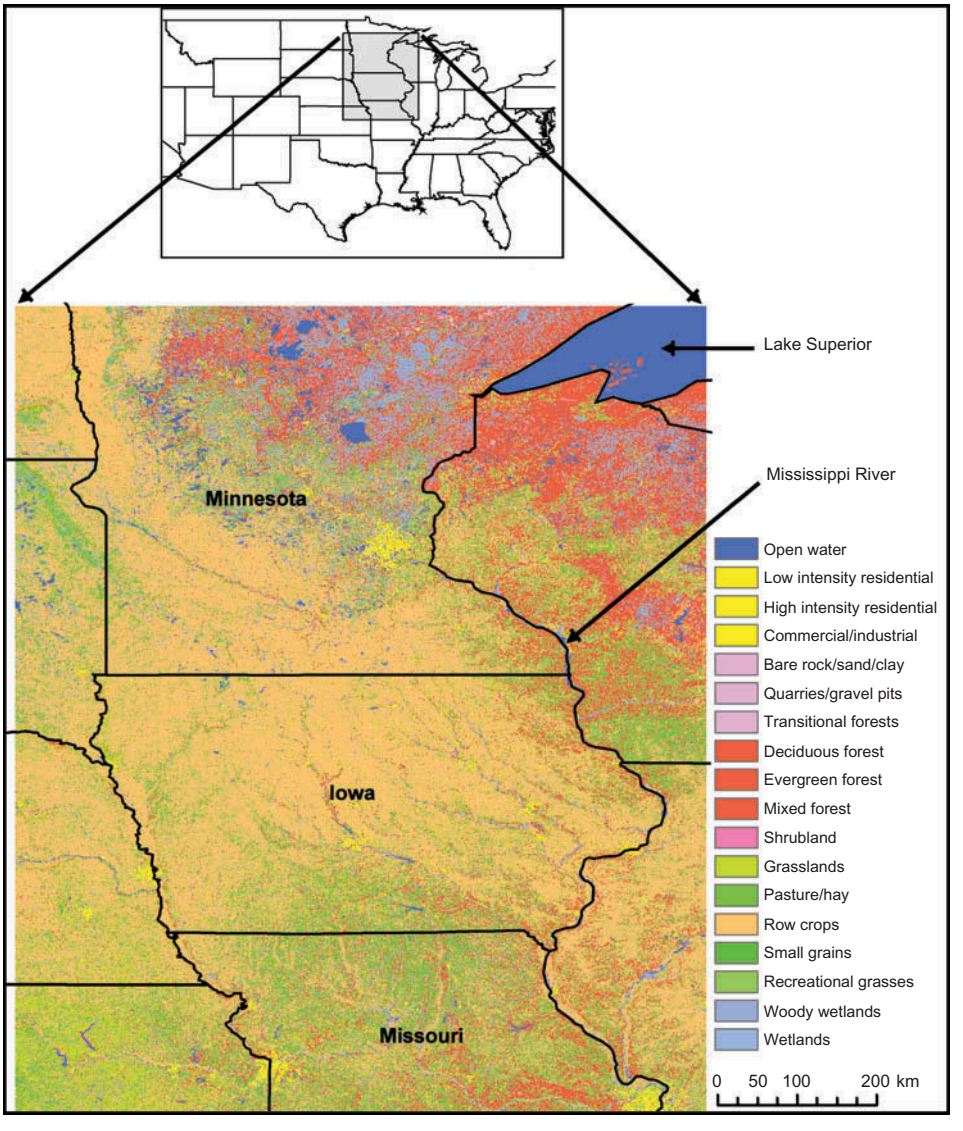

Figure 1. NLCD land-cover map of the study area.

small integration area for accurate representation of the underlying T_B heterogeneity. The microwave radiobrightness values assigned to the 1 km grid are hereafter referred to as the Original T_B ($T_{Original}$). Based on $T_{Original}$, we simulated SMAP point observations (L2A (Ashcroft and Wentz 2004)). SMAP is an L-band microwave radiometer planned to be launched in 2014 in a Sun synchronous orbit at 670 km altitude and at an effective Earth incidence angle of 40°. The L2A observations are anticipated to be separated by a nominal spatial distance of 10 km, much smaller than SMAP's anticipated average footprint size of 38 km, based on the specifications of the cancelled NASA mission Hydros (Crow et al. 2005). For this analysis, we assumed the Earth grid for the data of 40 km spatial resolution (similar to Crow et al. 2005), but this analysis can be performed for any similar Earth grid.

The $T_{Original}$, along with simulated SMAP footprint locations, was used in generating the T_B observations. Although the antenna response function in this article is assumed to be Gaussian in nature, the nature of the function is independent of the analysis since the function is explicitly introduced in the form of the G term in Equation (1). The Gaussian function is governed by the parameter σ^2, which can be determined by considering the 3 dB beamwidth equation (Limaye, Crosson, and Laymon 2006). Theoretically, the Gaussian response function has infinite extent, so in the interest of computational efficiency we chose to truncate the surface at 100 km radius, which accounts for over 99.6% of the total volume under a Gaussian surface. The simulated observations are without noise and thus theoretically ideal. However, sensor noise for SMAP is anticipated to be Gaussian with approximately 0.6 K, similar to the Hydros instrument (Crow et al. 2005). Therefore, this analysis includes white noise of this magnitude in our simulated observations.

To simulate realism in the synthetic observations, we created three T_B scenarios. All these scenarios are based on the NLCD data set, whereas the first one is a simple assignment of T_B value to a given land-cover class; this simulation is referred as the NLCD scenario. We added two more renditions of the NLCD, one called the Centre-minimum scenario. In this, we are simulating a rainfall event in the centre of the domain, whereby the T_B in the centre of the domain is lower than the edges. The transition from the centre to the edges is uniform in both longitudinal and latitudinal directions. The third scenario, called Gradient, simulates a T_B gradient from southeast to the northwest of the domain. For each of these scenarios, we convolved T_B using a range of sensor-noise standard deviation values. The range contains the 0.6 K instrument noise anticipated for SMAP instrument. Comparison of the BGM–ODC estimates with the CA method estimates for each of the noise levels and for each of the scenarios will present a complete picture of the efficacy of the BGM–ODC technique over the CA technique.

We used the assumed Gaussian antenna pattern at adjacent observation locations to estimate the a_i coefficients in Equation (4) in order to simulate BGM observations, as discussed earlier. The surface obtained by optimal estimation of the a_i coefficients (labelled BGM surface in Figure 2) shows the antenna pattern matching obtained using Equations (4) and (5) for the assumed Gaussian SMAP antenna pattern.

3. Results

We analysed errors for the noisy and BGM observations with respect to both the no-noise observations and the Earth grid. The noise added in observations is a result of the addition of Gaussian noise to the synthesized observations, whereas the noisy Earth grid T_B refers to the averaged value of the noise observations in a given Earth grid cell. BGM–ODC refers to the BGM observations used in the ODC estimation of Earth grid T_B.

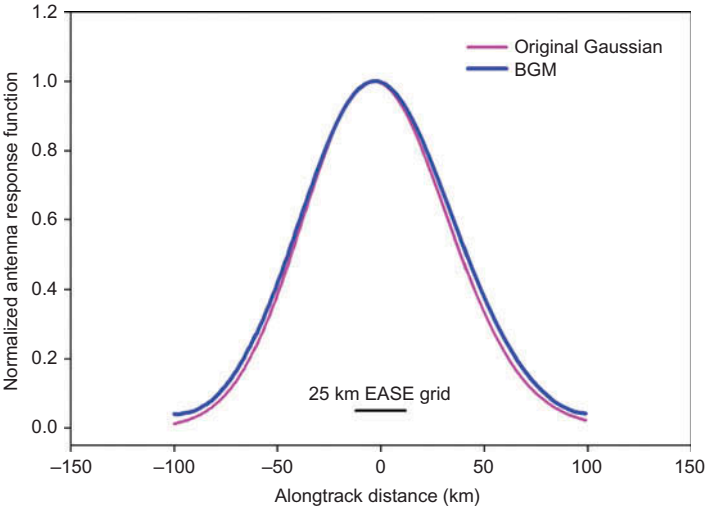

Figure 2. Antenna pattern matching for SMAP footprint geometry.

A comparison between SMAP-simulated data without sensor noise, data with sensor noise, and data treated with the BGM under the NLCD scenario is shown in Table 1. The no-noise data set is an accuracy benchmark for comparison with the two other observations, namely noisy and BGM. The mean and median T_B for both the benchmark and the noisy and BGM are similar. The root mean square error (RMSE) of the simulated data with injected noise is 0.6 K by definition, and this is borne out in the simulated data. The variance of the data set treated with BGM is slightly lower. Because the data set treated with BGM is a result of several adjacent noisy observations, the mean absolute error (MAE) and RMSE are lower in BGM observations than those in the data with noise.

BGM and noisy observations were used in deriving Earth grid T_B estimates. The ODC analysis performed on the BGM observations is referred as BGM–ODC Earth grid estimates, whereas the CA technique used in deriving the Earth grid T_B from noisy observations falling in each grid cell is referred as CA Earth grid estimates.

RMSE values for the three scenarios for the data sets after resampling to the Earth grid are shown in Table 2 for several levels of instrument noise standard deviations. For each scenario, the RMSE for the entire study area (labelled 'overall' in the table) is improved

Table 1. Comparison of observations among the three cases. Instrument noise with a SD of 0.6 K was added in the noisy and BGM cases.

Observations	No-noise	Noisy	BGM
Mean	270.66	270.67	270.66
Max	280.75	282.14	280.42
Min	177.1	177.28	178.96
Median	273.01	272.98	272.98
SD	11.79	11.79	11.58
MAE		0.48	0.26
RMSE		0.60	0.46
r^2		1.00	1.00

Table 2. Comparison of RMSE in Earth grid T_B for the ODC–BGM and CA techniques for the three T_B scenarios with respect to 'true' T_B for the entire domain ('Overall'), as well as the northern and southern halves.

		BGM–ODC			CA		
	SD	Overall	Northern	Southern	Overall	Northern	Southern
NLCD	0.4	2.285	3.144	0.731	4.614	6.448	0.962
	0.5	2.417	3.324	0.769	4.613	6.448	0.960
	0.6	**2.469**	**3.361**	**0.950**	**4.613**	**6.448**	**0.960**
	0.7	2.478	3.373	0.938	4.600	6.430	0.965
	0.8	2.510	3.417	0.955	4.608	6.440	0.961
	0.9	2.592	3.479	1.150	4.623	6.457	1.001
	1.0	2.477	3.308	1.140	4.612	6.443	0.987
		BGM–ODC			CA		
	SD	Overall	Northern	Southern	Overall	Northern	Southern
Gradient	0.4	2.402	3.315	0.719	4.682	6.551	0.922
	0.5	2.461	3.386	0.779	4.686	6.555	0.948
	0.6	**2.434**	**3.338**	**0.808**	**4.683**	**6.551**	**0.932**
	0.7	2.445	3.331	0.921	4.695	6.566	0.956
	0.8	2.384	3.245	0.908	4.683	6.550	0.949
	0.9	2.487	3.350	1.054	4.680	6.545	0.951
	1.0	2.554	3.434	1.130	4.689	6.558	0.943
		BGM–ODC			CA		
	SD	Overall	Northern	Southern	Overall	Northern	Southern
CentreMin	0.4	2.530	3.494	0.762	5.027	7.028	1.032
	0.5	2.481	3.402	0.849	5.036	7.040	1.044
	0.6	**2.627**	**3.607**	**0.866**	**5.048**	**7.056**	**1.057**
	0.7	2.628	3.613	0.873	5.031	7.034	1.037
	0.8	2.811	3.836	1.033	5.020	7.018	1.039
	0.9	2.729	3.683	1.153	5.049	7.058	1.043
	1.0	2.836	3.812	1.242	5.058	7.068	1.068

in the BGM–ODC case. The northern half of the study area contains numerous waterbodies whereas the southern half has agricultural crops and pastures which are relatively homogeneous in regard to T_Bs (Figure 1). In the northern half, for each scenario, the BGM–ODC estimates result in statistically significant improvement in MAE and RMSE. The BGM–ODC technique produces at least 40% improvement in RMSE compared with the CA technique under the anticipated 0.6 K SD instrument noise, shown as bold in Table 2. The improvements in RMSE are greater than that in MAE, suggesting that the BGM–ODC technique produced better estimates where the difference between the true and the estimates was high (resulting in larger squared errors).

In the southern half, the BGM–ODC technique produces about the same amount of errors as the CA method for 0.6 K SD instrument noise, with a slightly better performance in RMSE (shown in Table 2). As instrument noise increases (as reflected in SD increase), the accuracy of the BGM–ODC method worsens, falling below the CA method for instrument noise greater than 1 K SD.

In addition to the 0.4–1.0 K SD analysis presented in Table 2, we performed similar analysis for the 1.5 K SD noise case. The northern BGM–ODC results for the higher noise case show over 35% improvement in comparison with the CA technique, and nearly 18% worse performance in the southern half. Overall, the higher noise case shows similar trends to those presented in Table 2.

Figure 3 shows results for the NLCD scenario. The upper left panel is the original 1 km T_B for this scenario. The lower left is the mean of 1 km T_B for the simulated SMAP 40 km Earth grid cell and is referred to as the True T_B. The two middle panels show the BGM–ODC and CA T_B estimates. Comparing True T_B with ODC T_B (upper middle panel), it is clear that the spatial structure of T_B variability is better preserved in the BGM–ODC technique (upper middle) than in the CA technique (lower middle). The associated absolute errors are shown in the greyscale images in the two panels on the right. The MAE improvements in BGM–ODC T_B relative to the CA estimates are clear upon comparison of the two panels.

The ODC algorithm uses the subtle differences among the adjacent observations in relation to the shape of the response function to optimize for the Earth grid T_B. The errors added to the no-noise observations to produce the noisy observations are of the same orders of magnitude as the variations among the adjacent observations due to scene variation. Therefore, the ODC algorithm performs worse under high noise in observations in those parts of the study area where the T_B contrast is low (southern half). By comparison, in the northern parts of the study area, dominated by waterbodies, the BGM–ODC technique produces statistically superior T_B estimates.

This improvement comes with a cost, the added computational burden. The analysis requires solution of the system of simultaneous equations. For our study area, the ODC–BGM computations took several minutes (as compared to a few seconds for the CA technique). The time required for this technique will be a function of computer processor speeds, memory allocations for matrix manipulations, and compilers' options. That analysis is beyond the scope of this article, though a judicious analysis needs to be performed in order for a technique such as BGM–ODC to be operationally feasible.

4. Conclusions

Noise is inherent in microwave observations. Effects of noise are difficult to quantify in a real-world situation given the uncertainty of noise sources. We have taken a synthetic approach to this problem by creating microwave T_B using a forward radiobrightness model. The known Earth grid T_B was then convolved using an assumed Gaussian antenna response

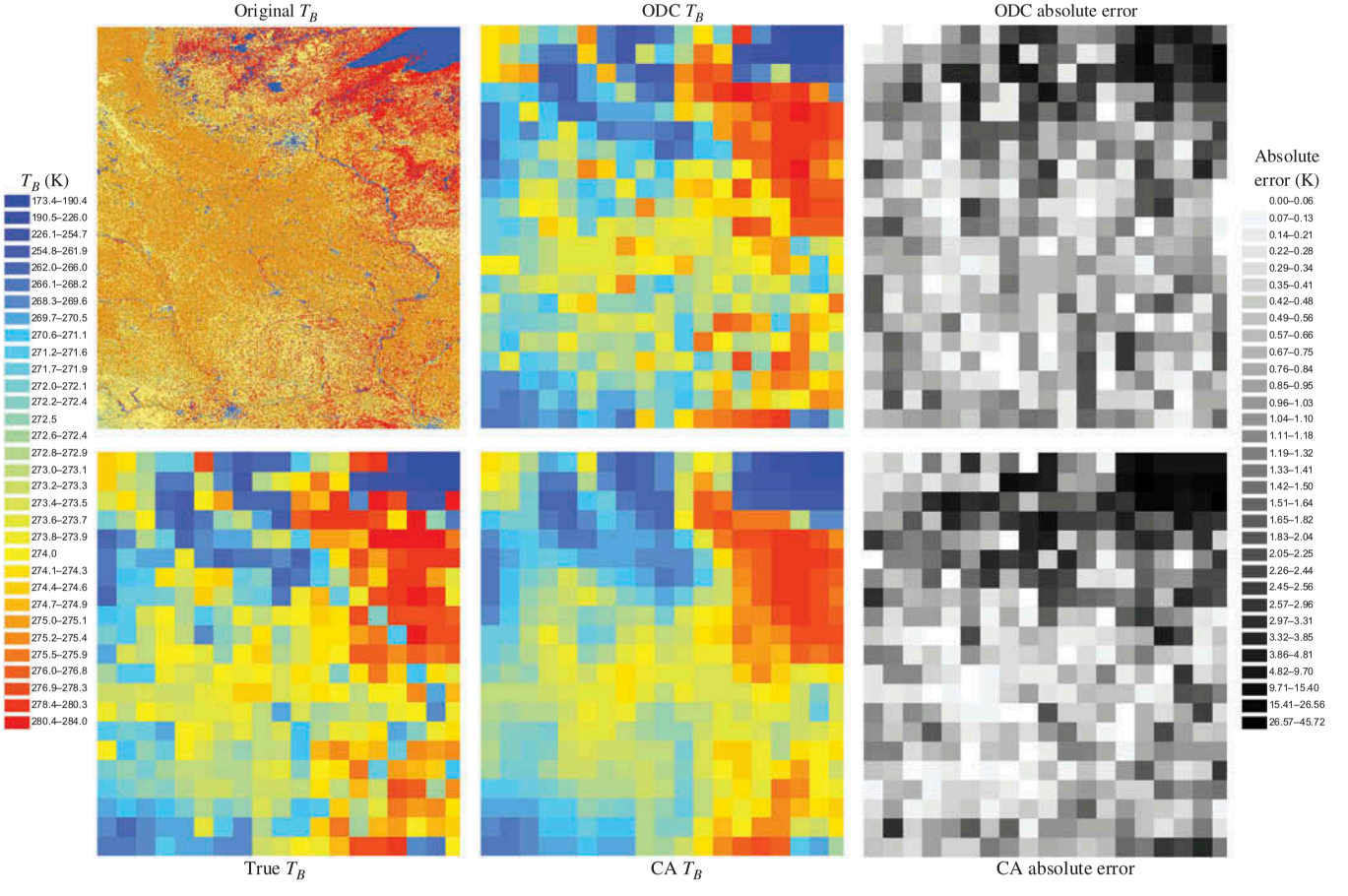

Figure 3. The results for the NLCD T_B scenario. Upper left: synthetic 1 km T_B. Lower left: synthetic T_B averaged to the 40 km Earth grid ('True' T_B). Upper centre: Earth grid T_B generated with the BGM–ODC method. Lower centre: Earth grid T_B generated with the CA method. Upper right: absolute difference between BGM–ODC and True T_B. Lower right: absolute difference between CA and True T_B.

function, though the technique presented here is independent of the form of that function. Our analyses with other antenna response functions have yielded similar results, so are omitted for the sake of brevity. Noise of known characteristics was then added to the simulated remotely sensed microwave observations. These observations are used to produce Earth grid T_B, which can be subsequently used in the retrieval of geophysical quantities such as soil moisture. We compared the two techniques with a noise-free data set; the conventional averaging of the noisy observations in each grid cell, and, second, an observation noise reduction technique (the Backus–Gilbert Method) followed by an ODC to produce Earth grid T_B. The results show that the latter technique produces over 40% improvement over the CA method in areas of high T_B contrast and comparable results in areas of lower T_B contrast under moderately noisy observations. Subtle differences among the adjacent observations are the result of varying emissions from the ground surface (non-random) and instrument noise (random). Our technique exploits the random nature of instrument noise to reduce error statistics. The CA technique does not distinguish among the sources of difference between adjacent observations. The BGM–ODC technique preserves the variations, while reducing the errors in the observations. The computational needs of this technique are higher because it requires simultaneous solution of a system of equations. The analysis of computational needs is beyond the scope of this work, but such an analysis will need to be performed for practical use of this technique.

References

Ashcroft, P., and W. Wentz. 2004. *AMSR-E/Aqua L2A Global Swath Spatially-Resampled Brightness Temperatures V002*. Boulder, CO: National Snow and Ice Data Centre. Digital media.

Bauer, P., and R. Bennartz. 1998. "Tropical Rainfall Measuring Mission Microwave Imaging Capabilities for the Observation of Rain Clouds." *Radio Science* 33: 335–349.

Bennartz, R. 2000. "Optimal Convolution of AMSU-B to AMSU-A." *Journal of Atmospheric and Oceanic Technology* 17: 1215–1225.

Crow, W. T., S. Chan, D. Entekhabi, A. Hsu, T. J. Jackson, E. Njoku, P. O'Neill, and J. Shi. 2005. "An Observing System Simulation Experiment for Hydros Radiometer-Only Soil Moisture and Freeze-Thaw Products." Proceedings of IEEE International Geoscience and Remote Sensing Symposium, IGARSS '05, Seoul, July 25–29. Vol. 4.

Farrar, M. R., and E. A. Smith. 1992. "Spatial Resolution Enhancement of Terrestrial Features Using Deconvolved SSM/I Microwave Brightness Temperatures." *IEEE Transactions on Geoscience and Remote Sensing* 30: 497–506.

Limaye, A. S., W. L. Crosson, and C. A. Laymon. 2006. "Estimating Accuracy in Optimal Deconvolution of Synthetic AMSR-E Observations." *Remote Sensing of Environment* 100: 133–142.

Limaye, A. S., W. L. Crosson, C. A. Laymon, and E. Njoku. 2004. "Land Cover-Based Optimal Deconvolution of PALS L-Band Microwave Brightness Temperatures." *Remote Sensing of Environment* 92: 497–506.

Mo, T. 1999. "AMSU-a Antenna Pattern Corrections." *IEEE Transactions on Geoscience and Remote Sensing* 37: 103–112.

Poe, G. A. 1990. "Optimum Interpolation of Imaging Microwave Radiometer Data." *IEEE Transactions on Geoscience and Remote Sensing* 28: 800–810.

Robinson, W. D., C. Kummerow, and W. S. Olson. 1992. "A Technique for Enhancing and Matching the Resolution of Microwave Measurements from the SSM/I." *IEEE Transactions on Geoscience and Remote Sensing* 30: 419–428.

Stephens, P. J., and A. S. Jones. 2002. "A Computationally Efficient Discrete Backus-Gilbert Footprint-Matching Algorithm." *IEEE Transactions on Geoscience and Remote Sensing* 40: 1865–1878.

Stephens, P. J., and A. S. Jones. 2007. "Geometrical Variations of Gain Patterns." *IEEE Transactions on Geoscience and Remote Sensing* 45: 376–382.

Stogryn, A. 1978. "Estimates of Brightness Temperatures from Scanning Radiometer Data." *IEEE Transactions on Antennas and Propagation [Legacy, Pre – 1988]* 26: 720–726.